RSC Advances

PAPER

Cite this: *RSC Adv.*, 2015, **5**, 39930

Exotic carbon nanostructures obtained through controllable defect engineering†

A. P. Sgouros,[abd] G. Kalosakas,*[abc] M. M. Sigalas[a] and K. Papagelis[ab]

Received 18th March 2015
Accepted 23rd April 2015

DOI: 10.1039/c5ra04831a

www.rsc.org/advances

We numerically demonstrate the spontaneous formation of various 3D carbon nanostructures, like multi-tube carbon nanotubes, nanopyramids, nanocubes, artificially rippled graphene, and other exotic nanomaterials, starting from graphene nanoribbons and inducing controllably engineered defects consisting of carbon adatoms or inverse Stone–Wales defects. The evolution of the initial defected planar structures towards the final 3D nanoarchitectures is obtained through molecular dynamics simulations, using different force fields to ensure the reproducibility of the derived results. The presented carbon nanostructures of different shapes, sizes, and morphologies, can be used in applications ranging from storage of hydrogen or other molecules, enhanced chemical reactions or catalysis in confined compartments, to drug delivery nanodevices and biosensors.

1. Introduction

There has been intense scientific research over the last decade into molecular traps enabling the capture and storage of small molecules such as methane, hydrogen, acetylene, and carbon dioxide. In particular, hydrogen as well as methane have properties that render them attractive fuels, but their storage presents substantial difficulties. Acetylene is an important building block in organic chemistry but its transportation is challenging because it should be stored in low pressure systems otherwise it becomes explosive. Finally, the increase of carbon dioxide in the atmosphere, mainly due to the combustion of gasoline and coal, is one of the greatest environmental problems and therefore searching for corresponding traps is an important issue. New classes of materials like the metal organic frameworks (MOFs) – crystalline porous materials consisting of metal oxides connected with organic compounds – have been suggested as promising molecular traps.[1–3] One of the main mechanisms for capturing small molecules in MOFs is physisorption, where the pores of the MOFs are chosen in such a way so to allow only certain size of gas molecules to pass through them. Carbon based materials, such as carbon nanotubes (CNTs),[4] fullerenes,[5] carbon nanoscrolls,[6] fullerene intercalated graphite,[7] and pillared graphene (composed of fused graphene layers and CNTs),[8] have been also suggested as promising hydrogen storage materials. These structures show significant increase of the hydrogen volumetric density by means of a simple physisorption mechanism. Moreover, by doping those structures with lithium cations, the hydrogen volumetric density can increase up to almost one order of magnitude.[4,8]

Functionalized carbon nanomaterials can also find important biomedical applications for drug delivery purposes, since they can serve as multi-functional formulations providing specific targeting, controlled delivery, and efficient treatment.[9] Recent works have demonstrated that functionalized graphene oxide,[10–15] as well as CNTs[16–18] can be successfully utilized in a number of examples as vehicles for controlled and targeted anticancer drug delivery. Similarly, other nanostructures, such as DNA origami,[19] are used as effective drug carriers too. Molecular traps and dams have been also suggested in other biological applications that will be able to miniaturize biosensors and bioanalytical systems;[20] it has been shown that nanoconstrictions with traps and dams can increase the local electric field several orders of magnitude resulting in much faster enrichment times for proteins than most reported methods.

Nanoscale compartments, apart from storage and delivery, may be also used for achieving improved kinetics of chemical reactions, as it is better exemplified by the nanopores in zeolites. Molecules confined in regions with dimensions of the order of the molecular size, exhibit different physical behavior compared to that in larger spaces, having implications in chemical reactions.[21] Except for the obvious cases where entropic effects are important, reactions involving large activation volume changes are also affected by confinement in nanocompartments. Further, shape selectivity, *i.e.* how the processed molecules (reactants, transition state, and products) fit in the confined area at the

[a]*Department of Materials Science, University of Patras, 26504 Patras, Greece. E-mail: georgek@upatras.gr*

[b]*Institute of Chemical Engineering Sciences – Foundation of Research and Technology Hellas (FORTH/ICE-HT), 26504 Patras, Greece*

[c]*Crete Center for Quantum Complexity and Nanotechnology (CCQCN), 71003 Heraklion, Greece*

[d]*School of Chemical Engineering, National Technical University of Athens (NTUA), 15780 Athens, Greece*

† Electronic supplementary information (ESI) available. See DOI: 10.1039/c5ra04831a

nanoscale, plays a crucial role for the occurrence of a successful transformation.[22] In that respect, deriving nanomaterials with various shapes can lead to controlled enhancement of particular chemical reactions at their interior.

The above mentioned applications would be advanced by proper engineering of nanostructures with various sizes and shapes, being closed or having specific openings on desire. We show that graphene nanoribbons (GNRs) with a spatially designed defect distribution can spontaneously form a large variety of stable 3D nanostructures, of controllable size and shape, on demand. The idea of such a control is based on the local bond distortion of the defected carbon atoms, resulting in well-defined bending of the graphene layer by ordered arrangements of defects, as it has been demonstrated by a number of molecular simulations.[23–26] This phenomenon of defect-induced graphene bending has been used for controlled construction of carbon nanoscrolls through programmable hydrogenation.[23] Further, properly placed hydrogen defects have driven the folding of a planar graphene structure towards the formation of a cubic nanocage, which is able to encapsulate a biomolecule.[24] Except for hydrogen, other individual atoms or chemical groups can similarly result in the bending of graphene sheets.[25]

We have shown that periodically placed defects, made by carbon atoms, in graphene nanoribbons can produce a variety of CNTs with different chiralities and sizes.[26] Based on the results of our recent works,[26,27] we report here the controllable formation of a large variety of 3D carbon nanostructures through proper engineering of carbon adatoms[28,29] or inverse Stone–Wales (ISTW) defects[30,31] in graphene. The obtained structures can be either simple polyhedra of various sizes at the nanoscale, or more exotic architectures. The folding of GNR with the use of ISTW defects has been also demonstrated with DFT calculations.[32]

We note that many steps for the development of realistic atomic defect fabrication methods are in progress. The fabrication of ribbons with sub-micrometer precision can be achieved experimentally with top-down[33] and bottom-up[34,35] approaches. Point defects such as atomic vacancies can be

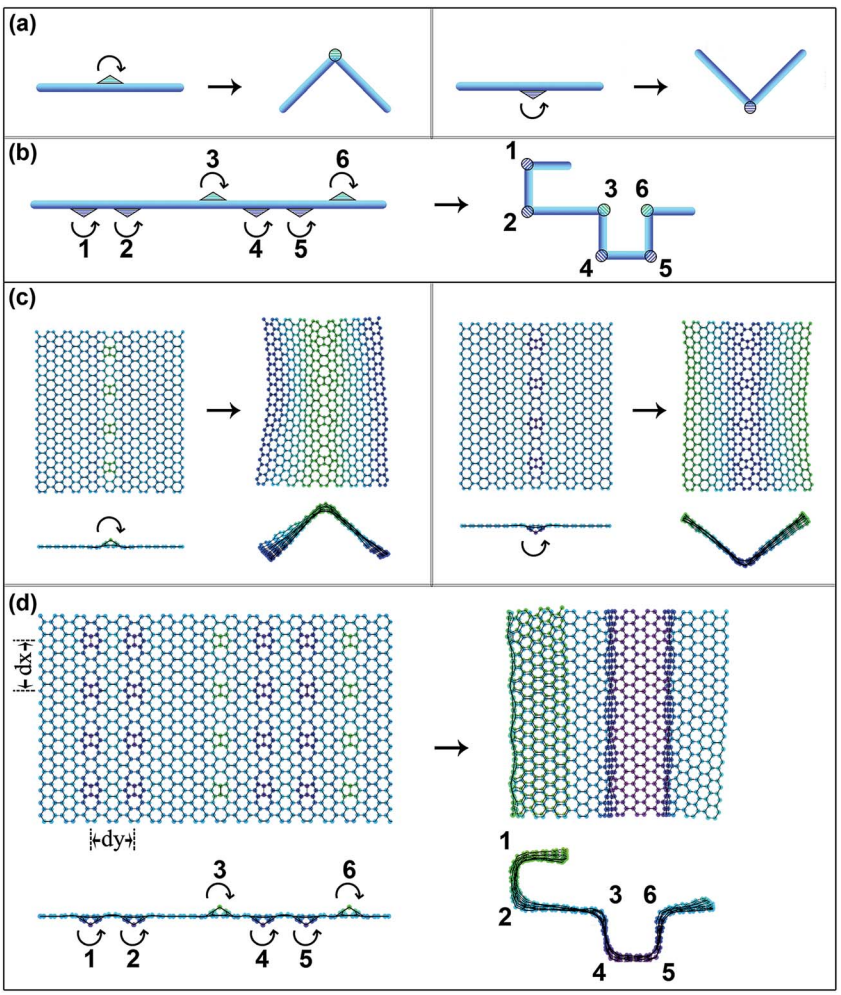

Fig. 1 Schematic representation of the transformation mechanism in GNRs. (a) By introducing single lines with type-A or type-B defects in the top/bottom of GNR, the graphene sheet can be inflected downwards/upwards. Thus, various nanostructures are generated in a controlled fashion, as shown from the side-view of the example (b). In (c) and (d) the configurations produced using molecular dynamics simulations are shown, for the corresponding cases schematically displayed in (a) and (b), respectively.

engineered with almost atomic resolution using highly focused electron beams.[36] Point defects such as carbon adatoms and inverse Stone–Wales defects (carbon dimers) can be produced with electron microscopy, ion irradiation and chemical methods.[37] At present the precise control of the exact location is rather challenging[37] though with the rapid technological advances this could be feasible in the future.

2. Methods

The molecular dynamics (MD) simulations were performed using LAMMPS code.[38] Two kinds of defects were considered: (i) carbon adatoms (referred as type-A defects); where single carbon atoms were inserted in-between neighboring carbon atoms and (ii) inverse Stone–Wales defects (referred as type-B defects); consisting of a pair of pentagonal carbon rings placed between a pair of heptagonal rings (see Fig. S1a and b in ESI† for a schematic representation of these two kinds of defects).[26] The pair-wise interactions were computed by applying either the Reactive Empirical Bond Order potential (REBO)[39] or the Tersoff's[40,41] potential for the C–C interactions. The results displayed below have been reproduced using both potentials and were visualized using the VMD package.[42] The MD simulations were performed within the framework of the canonical ensemble (NVT), with a fixed number of atoms N (ranging from 2000 to 10 000 in our simulations), constant volume V, constant temperature T (300 K) and a time step of 1 fs. The temperature of the system was maintained constant using the Nose–Hoover thermostat,[43,44] with a relaxation time span of 0.1 ps. At the edges of the simulation box, periodic boundary conditions were applied. In order to avoid spurious interactions along the edges of the simulation box, a large enough vacuum gap (~50 nm) was maintained, thus the GNR could move freely within the box. In order to stabilize the engineered defects within the GNR and dump the initial oscillations, we performed an energy minimization procedure for up to 10 ps at the beginning of each simulation. The obtained nanostructures were formed in a time scale ranging from 3 to 65 ps, depending on their size, shape and kind of defect used. In general, cases with type-A defects evolve slower than cases with type-B defects, since the latter ones correspond to higher inflection angles.[26]

3. Results

Fig. 1a illustrates the basic transformation mechanism of the GNR sheet, which has been extensively studied in a previous work.[26] Lines with type-A (adatoms) or type-B (ISTW) defects can be applied at the top (bottom) side of the GNR, resulting to downward (upward) inflection of the GNR. From now on, the application of lines with defects at the top (bottom) side of the GNR will be referred as ↑(↓). Most of the examples shown below have been obtained by using any type of defects (type-A or type-B).

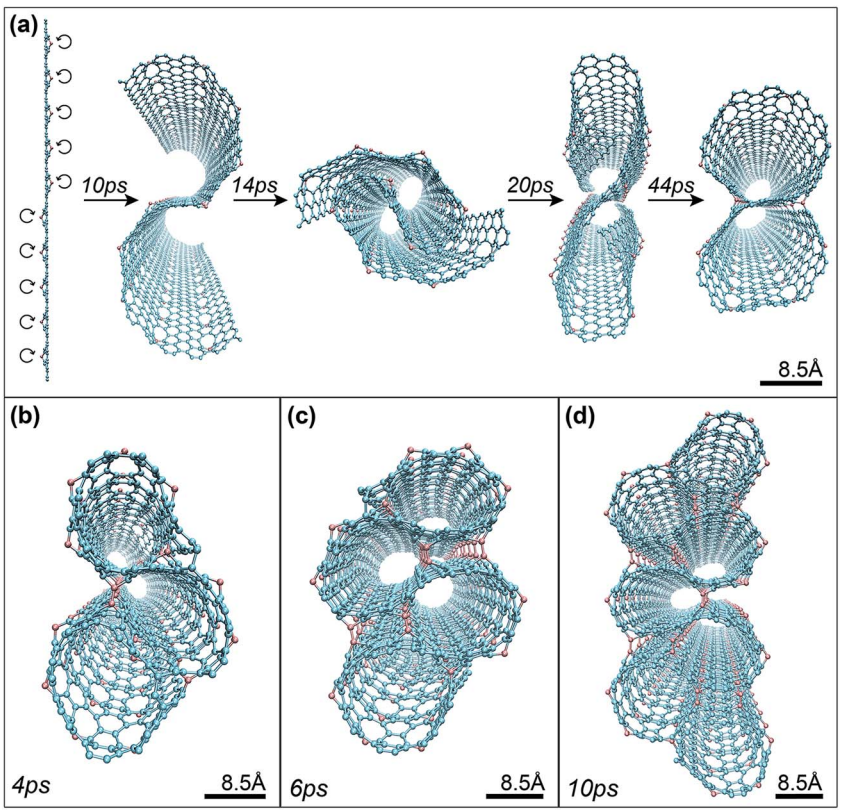

Fig. 2 Structures with multi-tube CNTs. (a) Snapshots displaying the transformation of a GNR to a double-tube CNT structure. Panels (b–d) display structures with (b) triple-tube, (c) quadruple-tube, and (d) septuple-tube CNTs. The corresponding time span and the length scale of each snapshot is also displayed.

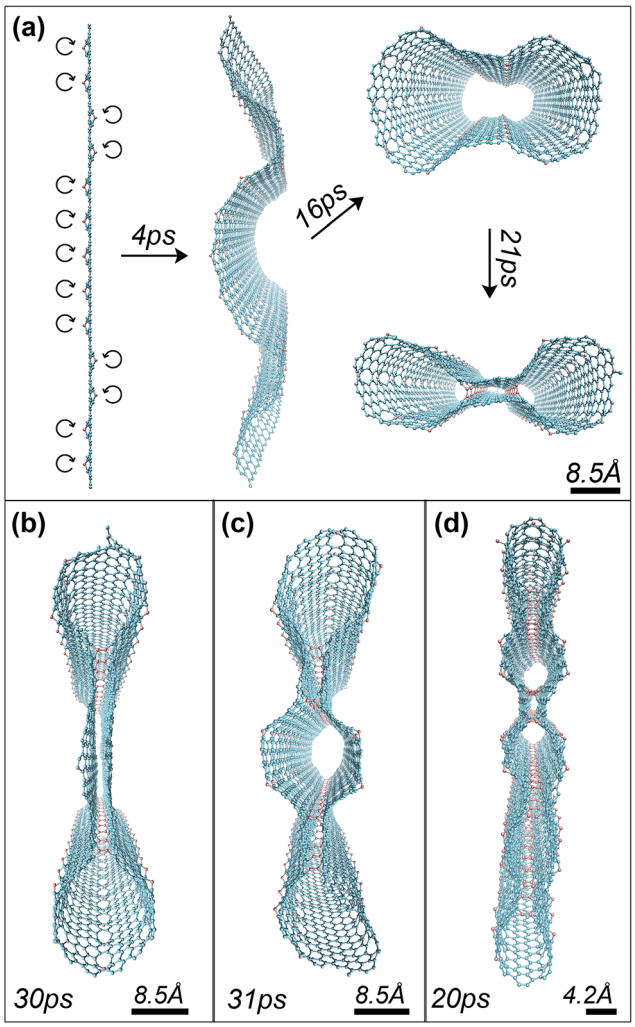

Fig. 3 Structures with multi-tube CNTs connected through GNR bilayers. (a) Snapshots displaying the evolution process of a GNR with type-A defects to a double-tube CNT structure. (b) A composite CNT–GNR bilayer structure. (c) A triple-tube CNT structure. (d) A quintuple-tube CNT structure.

By controllably applying the defect lines with ↑ and ↓ configurations in the GNRs, one can fabricate 3D nanostructures in various sizes and shapes (see Fig. 1b; the nanostructure with the equidistant configuration [↓↓-↑↓↓↑], where the "-" denotes the absence of a defect line). In Fig. 1c and d, the configurations shown schematically in Fig. 1a and b have been reproduced using MD simulations. In all cases shown below, the distance between the defect lines equals to $dy = 6a_{C-C}$ (= 8.5 Å), where a_{C-C} is the carbon–carbon equilibrium distance in graphene, while the distance separating the defects within the line equals to $dx = 4\sqrt{3}a_{C-C}$ (= 9.8 Å), except when otherwise is explicitly mentioned. Accordingly different (dx, dy) values give rise to similar results.[26]

Fig. 2 and 3 illustrate structures with multi-tube CNTs. In Fig. 2 the ↑ or ↓ configuration alternates every five consecutive defect lines, resulting in the folding of GNRs in structures with multi-tube CNTs (here, cases of double- up to seven-tube CNTs are shown). In Fig. 3 the resulted tubes are connected with small regions of bilayer graphene. The length of the connecting bilayer graphene region can be altered, as shown for example in Fig. 3b. An example with three tubes is shown in Fig. 3c. Another more exotic structure with five tubes, produced by the configuration $[(\uparrow\uparrow\downarrow\downarrow)_4\uparrow\uparrow\uparrow\uparrow(\downarrow\downarrow\uparrow\uparrow)_4]$ with $dy = 3a_{C-C}$ (= 4.3 Å) and $dx = 4\sqrt{3}a_{C-C}$ (= 9.8 Å), is presented in Fig. 3d. Multi-tubes with different radii can be formed as well by altering the density of the applied defects.[26]

Combined GNR–CNT structures can be also controllably engineered, with the GNRs connected either to the axial (see Fig. 4a and b) or the cylindrical (see Fig. 4c) side of CNTs. In Fig. 4a the GNR folds in particular regions towards the top side of the GNR, while in Fig. 4b the inflection alternates between the top and bottom sides of the GNR. Recently, similar intramolecular junctions of GNR and single-walled CNTs demonstrated experimentally, opening up possibilities for novel applications in graphene based electronics and optoelectronics.[45] In Fig. 4c the lines with the defects were applied at the edge of a long GNR, resulting in a CNT attached to a GNR nanostructure.

GNR with wave-like patterns can be produced by alternating regions of ↑ and ↓ configurations. For example, Fig. 5a shows the wave-like pattern produced by a repeated [↓↓↑↑] configuration of defect lines. Varying the distance between the defect lines and the configuration, the "wavelength" and the "amplitude" of the wave-like pattern can be controlled. This may enrich our techniques to formulate, manipulate and control ripples in graphene sheets, which strongly influence its electronic properties by inducing effective magnetic fields and modifying local potentials.[46,47] It is mentioned that wrinkled graphene has been successfully fabricated by synthesized

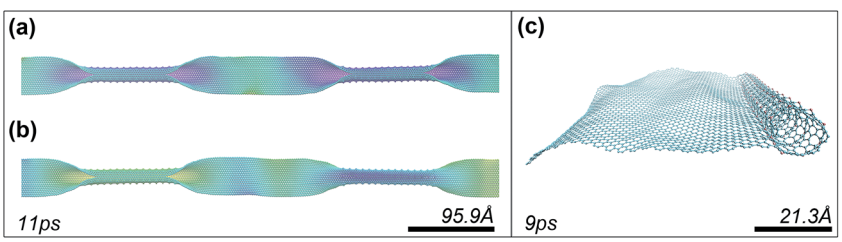

Fig. 4 Panels (a) and (b) display alternating GNR–CNT structures. In (a) the CNTs are obtained by upwards inflected GNRs, while in (b) GNRs are inflected upwards and downwards in an alternated fashion. (c) The edge of a GNR was properly inflected, resulting in a GNR–CNT hybrid material.

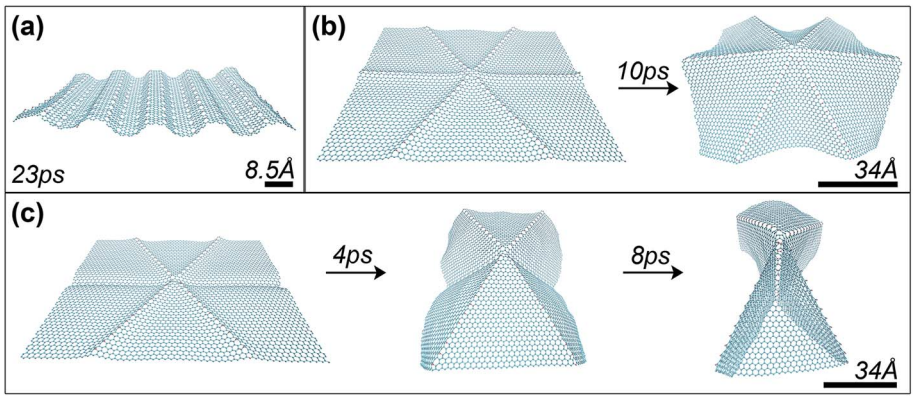

Fig. 5 (a) A wave-like GNR generated from a GNR with a repeated pattern ↓↓↑↑ of defects. (b) Introducing six lines with defects, forming 60° angle between each other, in the top of a GNR, a nano-umbrella structure is generated. (c) Similar to the aforementioned case, but two anti-diametric defect lines lie in the bottom instead of the top of the GNR; a twin-nanopyramid emerges.

graphene onto proper substrates having certain grating structure.[48] Designing defect lines with an angle of 60° between them, a structure resembling a nano-umbrella is produced (see Fig. 5b). This structure shares similarities with reported carbon nanocones,[49] while the flower like pattern has been observed experimentally in graphene trilayers grown on 6H–SiC substrate.[50] By changing the configuration of two anti-diametric lines in the case shown in Fig. 5b, the GNR transforms to two joined triangular nano-pyramids (see Fig. 5c).

Fig. 6a and c illustrate the evolution process of the transformation of GNRs with specific geometries and defect configurations to carbon nano-tetrahedrals and nano-cubes, respectively. In the latter case, a combination of both type-A and type-B defects is necessary. The volume of the obtained nanomaterials can be altered by orders of magnitude. For example, the tetrahedron (cube) of Fig. 6a (Fig. 6c) has a volume of 43 nm^3 (5 nm^3), while the volume of the corresponding structure shown in Fig. 6b (Fig. 6d) is 438 nm^3 (36 nm^3). For visual clarity an enlarged view of Fig. 6a is displayed in the ESI (Fig. S2†).

Furthermore, by properly manipulating the starting planar graphene segments (see Fig. S2†), the formation of nanopyramids with particular openings is possible, as opposed to the corresponding closed structures shown in Fig. 6a and b. Three such cases are illustrated in Fig. 7. A nano-tetrahedron with an open face (Fig. 7a) can be obtained either by lowering (or vanishing) the density of defects at the proper region of the face that is intended to stay open or by selectively manipulating a specific side of the initial triangular graphene segment (for example creating the small hole at the central part of a triangular side, as shown in Fig. S2†). Following a similar procedure (creating holes at the center of two out of the three sides of the initial triangular graphene) tetrahedrals with fully open edges can be created as well, as it is shown in Fig. 7b. Finally, by adding some extra atoms at the corresponding triangular side containing no hole at its center of the latter case, the size of the

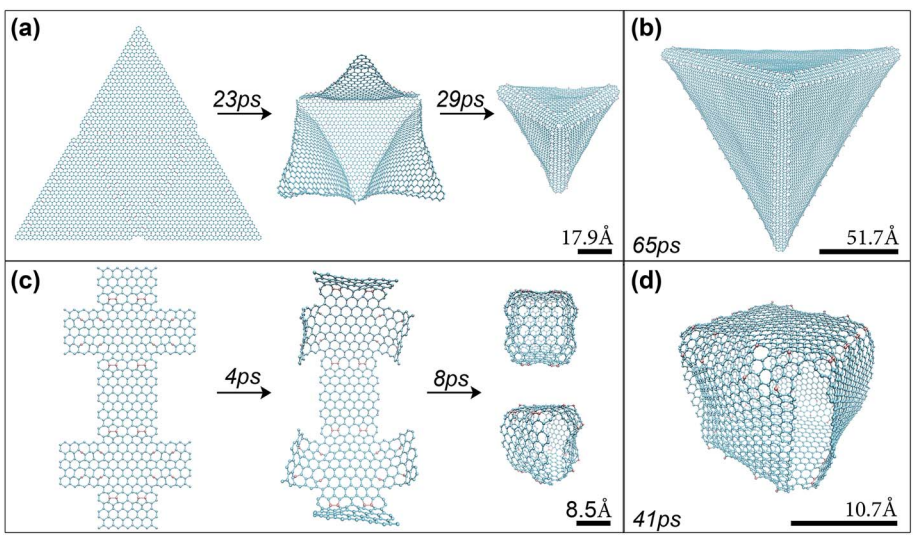

Fig. 6 Triangular nano-pyramids and nano-cubes. (a) and (c) display snapshots of the transformation process of GNRs, into a carbon tetrahedral and carbon nanocube, respectively. (b) and (d) display larger versions of (a) and (c), respectively.

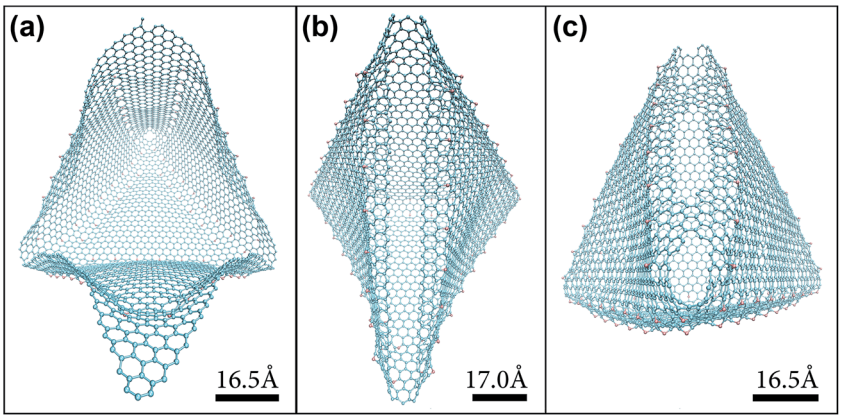

Fig. 7 Carbon nano-pyramids with (a) a completely open face, (b) an open edge, and (c) a partially open edge.

opening can be controlled, in order to obtain a partially open edge (Fig. 7c).

Animations that display the evolution process of the formed nanostructures shown in Fig. 2d, 3d, 5c, 6a, b and d are contained in the ESI.†

To obtain an idea of the energy barriers involved in the spontaneous transformations discussed here, we show in Fig. 8 the time course of the potential energy during the formation of the nanostructures presented in the cases of Fig. 2a, 3a and 6a (ignoring the energy minimization steps). A rise of the potential energy is observed at sub-picosecond time scales, where energy barriers of no more than 30–40 meV/atom are overcome. Then, the potential energy decreases and it stabilizes at times of the order of tens of ps. Note that, for the nano-pyramid shown in Fig. 6a, a rapid decline of the potential energy in Fig. 8 is clearly evident after about 20 ps, since many covalent bonds are formed during the development of the closed structure.

Concerning the stability and the potential mobility of the type-A (carbon adatoms) and type-B (carbon dimers) defects of the initially designed patterns in planar graphene, we note the following: the type-A defects have a binding energy of 1.5–2 eV (ref. 51 and 52) and a migration barrier equal to about 0.4 eV,[52] thus, they are in general mobile under ambient conditions.[37] In our simulations we did not observe any migrations of type-A defects. However, we mention that the presented nanostructures need about 3–65 ps to form, a time span that might be too small to observe such effects in samples containing 50–150 defect sites. To further verify this and in order to explore the possibility that this may be potentially due to inefficiencies of the used force fields, we performed some additional runs with the LcBOP[53] potential as well and we did not observe any migrations of adatoms. Regarding the type-B defects, they seem to be very stable and immobile at room temperature,[37] in accordance with our simulations where no migrations were observed. We finally note that most of our results can be reproduced with both types of defects, with some slight alterations of the patterns.

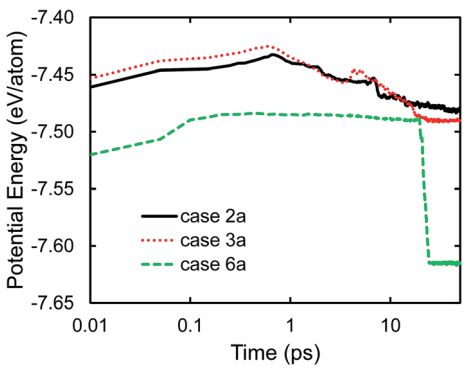

Fig. 8 The potential energy per atom as a function of the simulation time, for the formation of the nanostructures shown in cases 2a (solid line), 3a (dotted line) and 6a (dashed line).

4. Conclusions

By engineering defects in specific points of a GNR lattice with the desired configuration, we were able to produce various exotic nanomaterials such as: (i) multi-tube CNTs and closed or open nano-cages of various shapes and sizes, which may find applications in drug delivery, biosensors, enhancement of chemical reactions and in catalysis, (ii) artificially rippled graphene utilized in "strain engineering" concept of graphene and (iii) one dimensional GNR–CNT junctions exhibiting promising applications in logic gates, FETs and photodetectors.

Acknowledgements

This work has been partially supported by the GSRT grant 'Deformation, yield and failure of graphene and graphene-based nanocomposites' (ERC-10), co-financed by the European Union (ESF) and the Greek Ministry of Education (through ΕΣΠΑ program), and by European Union's Seventh Framework Programme (FP7-REGPOT-2012-2013-1) under grant agreement no. 316165.

References

1 S. L. James, Metal–organic frameworks, *Chem. Soc. Rev.*, 2003, **32**, 276–288.

2 R. B. Getman, Y. S. Bae, C. E. Wilmer and R. Q. Snurr, Review and analysis of molecular simulations of methane, hydrogen, and acetylene storage in metal–organic frameworks, *Chem. Rev.*, 2012, **112**, 703–723.

3 K. Sumida, D. L. Rogow, J. A. Mason, T. M. McDonald, E. D. Bloch, Z. R. Herm, T.-H. Bae and J. R. Long, Carbon Dioxide Capture in Metal–Organic Frameworks, *Chem. Rev.*, 2012, **112**, 724–781.

4 P. Chen, X. Wu, J. Lin and K. L. Tan, High H_2 Uptake by Alkali-Doped Carbon Nanotubes Under Ambient Pressure and Moderate Temperatures, *Science*, 1999, **285**, 91–93.

5 O. V. Pupysheva, A. A. Farajian and B. I. Yakobson, Fullerene Nanocage Capacity for Hydrogen Storage, *Nano Lett.*, 2008, **8**, 767–774.

6 G. Mpourmpakis, E. Tylianakis and G. E. Froudakis, Carbon Nanoscrolls: A Promising Material for Hydrogen Storage, *Nano Lett.*, 2007, **7**, 1893–1897.

7 A. Kuc, L. Zhechkov, S. Patchkovskii, G. Seifert and T. Heine, Hydrogen Sieving and Storage in Fullerene Intercalated Graphite, *Nano Lett.*, 2007, **7**, 1–5.

8 G. K. Dimitrakakis, E. Tylianakis and G. E. Froudakis, Pillared Graphene: A New 3-D Network Nanostructure for Enhanced Hydrogen storage, *Nano Lett.*, 2008, **8**, 3166–3170.

9 R. G. Mendes, A. Bachmatiuk, B. Buchner, G. Cuniberti and M. H. Rummeli, Carbon Nanostructures as Multi-Functional Drug Delivery Platforms, *J. Mater. Chem. B*, 2013, **1**, 401–428.

10 Z. Liu, J. T. Robinson, X. Sun and H. Dai, PEGylated Nanographene Oxide for Delivery of Water-Insoluble Cancer Drugs, *J. Am. Chem. Soc.*, 2008, **130**, 10876–10877.

11 X. Yang, X. Zhang, Z. Liu, Y. Ma, Y. Huang and Y. Chen, High-efficiency loading and controlled release of doxorubicin hydrochloride on graphene oxide, *J. Phys. Chem. C*, 2008, **112**, 17554–17558.

12 L. Zhang, J. Xia, Q. Zhao, L. Liu and Z. Zhang, Functional Graphene Oxide as a Nanocarrier for Controlled Loading and Targeted Delivery of Mixed Anticancer Drugs, *Small*, 2010, **6**, 537–544.

13 W. Zhang, Z. Guo, D. Huang, Z. Liu, X. Guo and H. Zhong, Synergistic effect of chemo-photothermal therapy using PEGylated graphene oxide, *Biomaterials*, 2011, **32**, 8555–8561.

14 D. Depan, J. Shah and R. D. K. Misra, Controlled release of drug from folate-decorated and graphene mediated drug delivery system: synthesis, loading efficiency, and drug release response, *Mater. Sci. Eng., C*, 2011, **31**, 1305–1312.

15 H. Bao, Y. Pan, Y. Ping, N. G. Sahoo, T. Wu, L. Li, Y. Li and L. H. Gan, Chitosan-Functionalized Graphene Oxide as a Nanocarrier for Drug and Gene Delivery, *Small*, 2011, **7**, 1569–1578.

16 J. Chen, S. Chen, X. Zhao, L. V. Kuznetsova, S. S. Wong and I. Ojima, Functionalized Single-Walled Carbon Nanotubes as Rationally Designed Vehicles for Tumor-Targeted Drug Delivery, *J. Am. Chem. Soc.*, 2008, **130**, 16778–16785.

17 S. Prakash, M. Malhotra, W. Shao, C. Tomaro-Duchesneau and S. Abbasi, Polymeric nanohybrids and functionalized carbon nanotubes as drug delivery carriers for cancer therapy, *Adv. Drug Delivery Rev.*, 2011, **63**, 1340–1351.

18 S. Peretz and O. Regev, Carbon nanotubes as nanocarriers in medicine, *Curr. Opin. Colloid Interface Sci.*, 2012, **17**, 360–368.

19 Q. Jiang, C. Song, J. Nangreave, X. Liu, L. Lin and D. Qiu, *et al.*, DNA Origami as a Carrier for Circumvention of Drug Resistance, *J. Am. Chem. Soc.*, 2012, **134**, 13396–13403.

20 K.-T. Liao and C.-F. Chou, Nanoscale Molecular Traps and Dams for Ultrafast Protein Enrichment in High-Conductivity Buffers, *J. Am. Chem. Soc.*, 2012, **134**, 8742–8745.

21 H. J. G. E. Gardeniers, Chemistry in nanochannel confinement, *Anal. Bioanal. Chem.*, 2009, **394**, 385–397.

22 B. Smit and T. L. M. Maesen, Towards a molecular understanding of shape selectivity, *Nature*, 2008, **451**, 671–678.

23 S. Zhu and T. Li, Hydrogenation enabled scrolling of graphene, *J. Phys. D: Appl. Phys.*, 2013, **46**, 075301.

24 L. Zhang, X. Zeng and X. Wang, Programmable hydrogenation of graphene for novel nanocages, *Sci. Rep.*, 2013, **3**, 3162.

25 M. Becton, L. Zhang and X. Wang, Effects of surface dopants on graphene folding by molecular simulations, *Chem. Phys. Lett.*, 2013, **584**, 135–141.

26 A. Sgouros, M. M. Sigalas, K. Papagelis and G. Kalosakas, Transforming graphene nanoribbons into nanotubes by use of point defects, *J. Phys: Condens. Matter*, 2014, **26**, 125301.

27 A. Sgouros, M. M. Sigalas, G. Kalosakas, K. Papagelis and N. I. Papanicolaou, Phononic band gap engineering in graphene, *J. Appl. Phys.*, 2012, **112**, 094307.

28 H. Amara, S. Latil, V. Meumier, P. Lambin and J.-C. Charlier, Scanning tunneling microscopy fingerprints of point defects in graphene: a theoretical prediction, *Phys. Rev. B: Condens. Matter Mater. Phys.*, 2007, **76**, 115423.

29 K. Nakada and A. Ishii, Migration of adatom adsorption on graphene using DFT calculation, *Solid State Commun.*, 2011, **151**, 13–16.

30 M. T. Lusk, D. T. Wu and L. D. Carr, Graphene nanoengineering and the inverse Stone–Thrower–Wales defect, *Phys. Rev. B: Condens. Matter Mater. Phys.*, 2010, **81**, 155444.

31 M. Sternberg, L. A. Curtiss, D. M. Gruen, G. Kedziora, D. A. Horner, P. C. Redfern and P. Zapol, Carbon Ad-Dimer Defects in Carbon Nanotubes, *Phys. Rev. Lett.*, 2006, **96**, 075506.

32 N. B. Le and L. M. Woods, Zigzag graphene nanoribbons with curved edges, *RSC Adv.*, 2013, **3**, 10014–10018.

33 F. Börrnert, L. Fu, S. Gorantla, M. Knupfer, B. Büchner and M. H. Rümmeli, Programmable sub-nanometer sculpting of graphene with electron beams, *ACS Nano*, 2012, **11**, 10327.

34 P. Han, K. Akagi, F. F. Canova, H. Mutoh, S. Shiraki, K. Iwaya, P. S. Weiss, N. Asao and T. Hitosugi, Bottom-up graphene-nanoribbon fabrication reveals chiral edges and enantioselectivity, *ACS Nano*, 2014, **8**, 9181–9187.

35 J. Cai, P. Reffieux, R. Jaafar, M. Bieri, T. Braun, S. Blankenburg, M. Muoth, A. P. Seitsonen, M. Saleh, C. Feng, K. Müllen and R. Fasel, Atomically precise bottom-up fabrication of graphene nanoribbons, *Nature*, 2010, **466**, 470–473.

36 R. Manzo and J. A. Banhart, Creation of individual vacancies in carbon nanotubes by using an electron beam of 1 Å diameter, *Nano Lett.*, 2009, **9**, 2285–2289.

37 F. Banhart, J. Kotakoski and A. V. Krasheninnikov, Structural defects in graphene, *ACS Nano*, 2011, **5**, 26–41.

38 S. Plimpton, Fast parallel algorithms for short-range molecular dynamics, *J. Comp. Physiol.*, 1995, **117**, 1–19.

39 S. J. Stuart, A. B. Tutein and J. A. Harrison, A reactive potential for hydrocarbons with intermolecular interactions, *J. Chem. Phys.*, 2000, **112**, 6472–6486.

40 J. Tersoff, New empirical approach for the structure and energy of covalent systems, *Phys. Rev. B: Condens. Matter Mater. Phys.*, 1988, **37**, 6991–7000.

41 J. Tersoff, Modeling solid-state chemistry: interatomic potentials for multicomponent systems, *Phys. Rev. B: Condens. Matter Mater. Phys.*, 1989, **39**, 5566–5569.

42 W. Humphrey, A. Dalke and K. Schulten, VMD: visual molecular dynamics, *J. Mol. Graphics*, 1996, **14**, 33–38.

43 S. Nosé, A unified formulation of the constant temperature molecular dynamics methods, *J. Chem. Phys.*, 1984, **81**, 511–519.

44 W. G. Hoover, Canonical dynamics: equilibrium phase-space distributions, *Phys. Rev. A*, 1985, **31**, 1695–1697.

45 D. Wei, L. Xie, K. K. Lee, Z. Hu, S. Tan, W. Chen, C. H. Sow, K. Chen, Y. Liu and A. T. S. Wee, Controllable unzipping for intramolecular junctions of graphene nanoribbons and single-walled carbon nanotubes, *Nat. Commun.*, 2012, **4**, 1374.

46 W. Bao, F. Miao, Z. Chen, H. Zhang, W. Jang, C. Dames and C. N. Lau, Controlled ripple texturing of suspended graphene and ultrathin graphite membranes, *Nat. Nanotechnol.*, 2009, **4**, 562–566.

47 F. Guinea, M. I. Katsnelson and A. K. Geim, Energy gaps and a zero-field quantum Hall effect in graphene by strain, *Nat. Phys.*, 2010, **6**, 30–33.

48 P. Zhonghuai, L. Nan, F. Lei and L. Zhongfan, Wrinkle engineering: a new approach to massive graphene nanoribbon arrays, *J. Am. Chem. Soc.*, 2011, **133**, 17578–17581.

49 S. N. Naesswall, A. Elgsaeter, G. Helgesen and K. D. Knudsen, Carbon nanocones: wall structure and morphology, *Sci. Technol. Adv. Mater.*, 2009, **10**, 065002.

50 B. Lalmi, J. C. Girard, E. Pallecchi, M. Silly, C. David, S. Latil, F. Sirotti and A. Ouerghi, Flower-shaped domains and wrinkles in trilayer epitaxial graphene on silicon carbide, *Sci. Rep.*, 2014, **4**, 4066.

51 Y. H. Lee, S. G. Kim and D. Tomanek, Catalytic growth of single-wall carbon nanotubes: an *ab initio* study, *Phys. Rev. Lett.*, 1997, **78**, 2393–2396.

52 P. O. Lehtinen, A. S. Foster, A. Ayuela, A. Krasheninnikov, K. Nordlund and R. M. Nieminen, Magnetic properties and diffusion of adatoms on a graphene sheet, *Phys. Rev. Lett.*, 2003, **91**, 017202.

53 J. H. Los and A. Fasolino, Intrinsic long-range bond-order potential for carbon: performance in Monte Carlo simulations of graphitization, *Phys. Rev. B: Condens. Matter Mater. Phys.*, 2003, **68**, 024107.